Journal of Solid State Chemistry 183 (2010) 920–926

Contents lists available at ScienceDirect

Journal of Solid State Chemistry

journal homepage: www.elsevier.com/locate/jssc

$Yb_5Ni_4Sn_{10}$ and $Yb_7Ni_4Sn_{13}$: New polar intermetallics with 3D framework structures

Xiao-Wu Lei [a,b], Zhong-Ming Sun [a,b], Long-Hua Li [a,b], Guo-Hua Zhong [a], Chun-Li Hu [a], Jiang-Gao Mao [a,*]

[a] State Key Laboratory of Structural Chemistry, Fujian Institute of Research on the Structure of Matter, Chinese Academy of Sciences, Fuzhou 350002, PR China
[b] Graduate School of the Chinese Academy of Sciences, Beijing 100039, PR China

ARTICLE INFO

Article history:
Received 10 December 2009
Received in revised form
28 January 2010
Accepted 6 February 2010
Available online 16 February 2010

Keywords:
Polar intermetallics
Solid-state reactions
Crystal structures
Stannides
Electronic structure calculations

ABSTRACT

The title compounds have been obtained by solid state reactions of the corresponding pure elements at high temperature, and structurally characterized by single-crystal X-ray diffraction studies. $Yb_5Ni_4Sn_{10}$ adopts the $Sc_5Co_4Si_{10}$ structure type and crystallizes in the tetragonal space group *P4/mbm* (No. 127) with cell parameters of a=13.785(4) Å, c=4.492 (2) Å, V=853.7(5) Å^3, and Z=2. $Yb_7Ni_4Sn_{13}$ is isostructural with $Yb_7Co_4InGe_{12}$ and crystallizes in the tetragonal space group *P4/m* (No. 83) with cell parameters of a=11.1429(6) Å, c=4.5318(4) Å, V=562.69(7) Å^3, and Z=1. Both structures feature three-dimensional (3D) frameworks based on three different types of one-dimensional (1D) channels, which are occupied by the Yb atoms. Electronic structure calculations based on density functional theory (DFT) indicate that both compounds are metallic. These results are in agreement with those from temperature-dependent resistivity and magnetic susceptibility measurements.

1. Introduction

Ternary *RE*–*TM*–Sn phases (*RE*=rare earth metal, *TM*=transition metal) have been extensively investigated in recent years due to their richness in structural chemistry and tunable electronic properties [1–3]. The Sn-rich phases exhibit various polyanionic Sn-based substructures such as clusters, chains, rings and nets with a wide range of Sn–Sn bonding interactions [4–14]. These compounds display interesting physical properties due to either RE or TM substructure, or both, such as large magnetoresistance (e.g., $REMn_6Sn_6$) [15], superconductivity phenomena (e.g., $RE_3TM_4Sn_{13}$, *TM*=Rh, Co) [16], and Kondo behavior (e.g., $Ce_3Cu_4Sn_4$) [17].

The investigation of RE–Ni–Sn system has afforded a variety of ternary phases with diversiform structures and tuned physical properties [18–26]. For example, the equiatomic RENiSn features a 3D anionic network composed of 1D [NiSn] ladders interconnected via Ni–Sn bonds, which show the potential applications in hydrogen storage [18,19]. The structures of $RENi_2Sn_2$ (*RE*=La–Nd, Sm, Gd) with $CeAl_2Ga_2$ type feature a 3D framework based on 2D corrugated [NiSn] layers [20–21]. With a higher tin content, stannides such as $RENiSn_2$ (*RE*=La–Nd), $RENiSn_4$ (*RE*=Gd–Tm, Lu), Sm_2NiSn_4, $RE_3Ni_2Sn_7$ (*RE*=La, Ce) and Lu_2NiSn_6 have been isolated [22–26]. In most of these phases, Sn atoms tend to form [Sn_4] squares, which are completely or partially capped by Ni atoms to form various types of 2D layers. These layers are interconnected or separated by zigzag Sn chains into diverse structures. In addition, $Gd_3Ni_8Sn_{16.33}$, $Dy_4Ni_{12}Sn_{25}$, $La_{4.87}Ni_{12}Sn_{24}$, and $RE_9Ni_{24}Sn_{49}$ (*RE*=Y, La–Nd, Sm, Gd, Tb) have also been reported with abundant physical properties [27–30]. It should be noted that the rare earth atoms play an important role in the modulation of structures and physical properties of the compounds. For example, $RENiSn_2$ (*RE*=Tb, Dy, Ho) are not isostructural with $RENiSn_2$ (*RE*=La–Nd) ($CeNiSi_2$ type), but crystallizes in a new structure type due to the effect of the lanthanide contraction [31].

Among these ternary stannides, the Yb phases are particularly of research interest because Yb can exhibit two valence states concerning the nonmagnetic $4f^{14}$ (Yb^{2+}) and magnetic $4f^{13}$ (Yb^{3+}) electronic configurations [32,33], which may stabilize novel polyanionic frameworks that are unknown for other lanthanide metals. So far, only a few Yb–Ni–Sn ternary phases have been reported: YbNiSn (TiNiSi structure type, *Pnma*) [34], $YbNi_{2-x}Sn$ ($P6_3/mmc$) [35], $YbNi_2Sn$ ($MgCu_2Al$ structure type, *Fm*-3*m*) [36], $Yb_{1-x}Ni_4Sn_{1+x}$ ($MgCu_4Sn$ structure type, *F*-43*m*) [37], and $YbNi_{5-x}Sn_{1+x}$ ($CeCu_{4.38}In_{1.62}$ structure type, *Pnnm*) [38]. Our systematic explorations in this system led to two new members, namely, $Yb_5Ni_4Sn_{10}$ and $Yb_7Ni_4Sn_{13}$. Their structures feature two types of 3D frameworks based on 1D [Ni_4Sn_8] chains composed of "drum"-shaped [Ni_4Sn_{12}] cages. Herein, we report their syntheses, crystal structures, chemical bonding, and properties.

2. Experimental section

2.1. Materials and instrumentation

All manipulations were performed within an argon-filled glove box with moisture level below 1 ppm. All starting materials were

* Corresponding author. Fax: +86 591 83704836.
E-mail address: mjg@fjirsm.ac.cn (J.-G. Mao).

0022-4596/$ - see front matter © 2010 Elsevier Inc. All rights reserved.
doi:10.1016/j.jssc.2010.02.004

used as received: Yb blocks (Acros, 99.99%), Ni powder (Tianjin Fuchen chemical reagent company, 99.99%), Sn granules (Acros, 99.99%). Semi-quantitative microprobe elemental analyses for Yb, Ni and Sn were performed on a JSM-6700F scanning electron microscope (SEM) equipped with an energy dispersive spectroscope (EDS) detector. X-ray diffraction (XRD) powder patterns were collected at room temperature on a X'Pert-Pro diffractometer using Cu$K\alpha$ radiation (λ=1.5406 Å) in the 2θ range of 5–85° with a step size of 0.04° and 10 s/step counting time. Magnetic susceptibility measurements were performed on a Quantum Design PPMS-9T magnetometer in the temperature range of 5–300 K. The polycrystalline samples of the title compounds were ground to a fine powder to minimize possible anisotropic effects and loaded into a gelatin capsule. The samples were cooled in a constant magnetic field of 5000 Oe for measurements of magnetization versus temperature. The powder samples were cold-pressed into $3.0\times3.0\times7.0$ mm bar-shaped model for resistivity measurements, which were performed on an Oxford Mablab-12 magnetometer using a standard four-probe technique in the temperature range of 5–300 K.

2.2. Preparation of $Yb_5Ni_4Sn_{10}$ and $Yb_7Ni_4Sn_{13}$

Single crystals of $Yb_5Ni_4Sn_{10}$ and $Yb_7Ni_4Sn_{13}$ were initially obtained from the solid state reactions of the mixture of Yb, Ni and Sn metals in molar ratio of 1:1:3 and 2:1:3, respectively. The samples were loaded into tantalum tubes, which were subsequently arc-welded under argon atmosphere and sealed in the quartz tube under vacuum ($\sim10^{-4}$ Torr). The quartz tubes were put into high-temperature furnace and allowed to react at 980 °C for 6 days, and then they were allowed to cool at a rate of 0.1 °C/min to room temperature. The prism-shaped single crystals of $Yb_5Ni_4Sn_{10}$ and $Yb_7Ni_4Sn_{13}$ were respectively selected for structural analysis. Microprobe elemental analyses on clean surfaces of several single crystals gave approximate Yb:Ni:Sn molar ratios of 5.0(8):4.3(5):10.4(6) and 7.0(8):3.8(7):13.4(6) for $Yb_5Ni_4Sn_{10}$ and $Yb_7Ni_4Sn_{13}$, respectively, which were in agreement with the results derived from single crystal X-ray diffraction refinements. Subsequently, the reactions were carried out with the stoichiometric mixture of the corresponding elements. The samples were heated at 980 °C for 2 days, and then annealed at 670 °C for 15 days (for $Yb_5Ni_4Sn_{10}$) and 600 °C for 10 days (for $Yb_7Ni_4Sn_{13}$), respectively. The measured X-ray diffraction powder patterns agree well with those simulated from the single-crystal X-ray structural analysis (See Supplementary materials). Attempts to synthesize other lanthanide analogs (La, Sm, Eu, Dy, Er, and Lu) were tried but were unsuccessful.

2.3. Crystal structure determination

Single crystals of $Yb_5Ni_4Sn_{10}$ and $Yb_7Ni_4Sn_{13}$ were selected from the reaction products and sealed into thin-walled glass capillaries within the glove-box. Data collections for the title compounds were performed on a Rigaku Mercury CCD (Mo$K\alpha$ radiation, graphite monochromator) at 293(2) K. Both data sets were corrected for Lorentz factor, polarization, air absorption and absorption due to variations in the path length through the detector faceplate. Absorption corrections based on multi-scan method were also applied [39].

Both the structures were solved using direct methods (SHELX-97) which revealed all atomic positions, and refined by least-squares methods with atomic coordinates and anisotropic thermal parameters [40]. For $Yb_5Ni_4Sn_{10}$, inspection of the systematic absences for the full data set indicated the possible space group to be *P*4/*mbm* (No. 127), *P*-4*b*2 (No. 117), and *P*4*bm* (No. 100), of which the centrosymmetric one gave a satisfactory refinement. The space group for $Yb_7Ni_4Sn_{13}$ was *P*4/*m* (No. 83) based on systematic absences, E-value statistics and satisfactory refinements. Site occupancy refinements for $Yb_5Ni_4Sn_{10}$ and $Yb_7Ni_4Sn_{13}$ indicated that all sites were fully occupied. Final difference Fourier maps showed featureless residual peaks of 1.72 e/Å^3 (0.84 Å from the Yb(1) atom) and −2.62 e/Å^3 (0.70 Å from the Yb(3) atom) for $Yb_5Ni_4Sn_{10}$; 1.49 e/Å^3 (0.87 Å from Yb(2) atom) and −1.36 e/Å^3 (1.32 Å from Yb(2) atom) for $Yb_7Ni_4Sn_{13}$, respectively. Data collection and refinement parameters for the two compounds are summarized in Table 1. Atomic coordinates and important bond lengths are listed in Tables 2 and 3, respectively.

Crystallographic data in CIF format for $Yb_5Ni_4Sn_{10}$ and $Yb_7Ni_4Sn_{13}$ have been given as Supplementary materials. These data can also be obtained from the Fachinformationszentrum Karlsruhe, 76344 Eggenstein-Leopoldshafen, Germany, (fax: +49 7247 808 666; e-mail: crysdata@fiz-karlsruhe.de) on quoting the depository numbers CSD 420765 and 420766.

Table 1
Crystal Data and Structure Refinements for $Yb_5Ni_4Sn_{10}$ and $Yb_7Ni_4Sn_{13}$.

Chemical formula	$Yb_5Ni_4Sn_{10}$	$Yb_7Ni_4Sn_{13}$
fw	2286.94	2989.09
Space group	*P*4/*mbm* (No. 127)	*P*4/*m* (No. 83)
a (Å)	13.785(4)	11.1429(6)
b (Å)	13.785(4)	11.1429(6)
c (Å)	4.492(2)	4.5318(4)
V (Å^3)	853.7(5)	562.69(7)
Z	2	1
Crystal size (mm)	$0.45\times0.05\times0.05$	$0.10\times0.05\times0.05$
Temperature (K)	293	293
D_{calcd} (g cm^{-3})	8.897	8.821
h k l ranges	±17, ±17, ±5	±14, (−14, 13), ±5
μ (mm^{-1})	45.658	46.102
Reflections collected	6498	4398
Unique reflections	586	732
Reflections ($I>2\sigma(I)$)	554	667
GOF on F^2	1.199	1.146
*R*1, *wR*2 ($I>2\sigma(I)$)[a]	0.0237/0.0534	0.0218/0.0425
*R*1, *wR*2 (all data)	0.0254/0.0542	0.0260/0.0437

[a] $R1=\sum||F_o|-|F_c||/\sum|F_o|$, $wR2=\{\sum w[(F_o)^2-(F_c)^2]^2/\sum w[(F_o)^2]^2\}^{1/2}$.

Table 2
Atomic coordinates and equivalent displacement parameters ($\times10^3$ Å^2) for $Yb_5Ni_4Sn_{10}$ and $Yb_7Ni_4Sn_{13}$.

Atom	Wyck	*x*	*y*	*z*	*U*(eq)[a]
$Yb_5Ni_4Sn_{10}$					
Yb(1)	2*a*	1/2	1/2	0	7(1)
Yb(2)	4*h*	0.6791(1)	0.1791(1)	1/2	8(1)
Yb(3)	4*h*	0.3924(1)	0.1076(1)	1/2	10(1)
Ni(1)	8*i*	0.7553(1)	0.0323(1)	0	7(1)
Sn(1)	8*i*	0.8499(1)	0.1993(1)	0	8(1)
Sn(2)	8*j*	0.8355(1)	0.0097(1)	1/2	8(1)
Sn(3)	4*g*	0.5718(1)	0.0718(1)	0	7(1)
$Yb_7Ni_4Sn_{13}$					
Yb(1)	1*c*	1/2	1/2	0	7(1)
Yb(2)	4*k*	0.8390(1)	0.8291(1)	1/2	8(1)
Yb(3)	2*f*	0	1/2	1/2	11(1)
Ni(1)	4*j*	0.6201(1)	0.7760(1)	0	9(1)
Sn(1)	4*j*	0.7847(1)	0.6107(1)	0	9(1)
Sn(2)	4*k*	0.5767(1)	0.6906(1)	1/2	9(1)
Sn(3)	4*j*	0.7153(1)	0.9814(1)	0	8(1)
Sn(4)	1*a*	0	0	0	9(1)

[a] *U*(eq) is defined as one-third of the trace of the orthogonalized U_{ij} tensor.

2.4. Electronic structure calculations

To better understand the chemical bonding of the title compounds, *ab initio* electronic structure calculations were performed with both the full-potential linearized augmented plane wave plus the local basis (FPLAPW+lo) method (WIEN2 K) and tight-binding linear muffin-tin orbital (TB–LMTO–ASA) method.

WIEN2K: The WIEN2K program is based on the density functional theory (DFT) and FPLAPW+lo method, using the general gradient approximation (GGA-PBE) to treat the exchange and correlation potential [41–44]. Within the FPLAPW method, the space is divided into nonoverlapping muffin-tin (MT) spheres and interstitial region. The parameter $R_{MT} \times K_{MAX}$ (R_{MT} is the smallest muffin-tin spherical radius present in the system, and K_{MAX} is the maximum modulus for the reciprocal lattice vector) is used to determine the number of plane waves needed for the expansion of the wave function in the interstitial region. Here, we adopted the values of 2.5, 2.5, and 2.23 a.u. for Yb, Ni and Sn atoms, respectively, as the R_{MT} radii and let $R_{MT} \times K_{MAX}$=7. In addition, a separate energy −8.0 *Ry* between valence and the core states was used. Thus, the Yb-4*f*5*d*6*s*, Ni-3*d*4*s*, and Sn-5*s*5*p* orbitals were treated as valence states. Self-consistency calculation of electronic structures was achieved when the total-energy variation from iteration to iteration converged to 0.01 mRy accuracy or better. We calculated the total energy and magnetic moments with 100, 200, and 500 *k*-points for both compounds, and the results suggested that the calculated results did not change much from 100 to 500 *k*-points. Hence in this study, we used the 200 *k*-point in the complete Brillouin zone, and the Brillouin zone integration was carried out with a modified tetrahedron method [45]. The Fermi level was selected as the energy reference (E_F=0 eV).

Stuttgart LMTO Program: This program follows the TB–LMTO–ASA method in the local density and atomic sphere (ASA) approximations [46–49]. Exchange and correlation were treated in the local density approximation (LDA) [50]. Interstitial spheres were introduced in the last to achieve space filling. The ASA radii as well as the positions and radii of additional empty spheres were calculated automatically. The basis set included the 6*s*, 6*p*, 5*d*, and 4*f* orbitals for Yb; 4*s*, 4*p*, 3*d*, and 3*f* orbitals for Ni; and 5*s*, 5*p*, 4*d*, and 4*f* orbitals for Sn atoms. The Yb 6*p*, Ni 3*f*, 4*p*, and Sn 4*d*, 4*f* orbitals were treated with the down-folding technique [51–53]. In both cases, the *k*-space integrations were performed by the tetrahedron method [45]. The Fermi level was selected as the energy reference (E_F=0 eV).

Table 3
Important bond lengths (Å) for $Yb_5Ni_4Sn_{10}$ and $Yb_7Ni_4Sn_{13}$.

$Yb_5Ni_4Sn_{10}$					
Yb(1)–Sn(1)	3.439(1)	×4	Yb(3)–Sn(1)	3.533(1)	×4
Yb(1)–Sn(2)	3.1947(9)	×8	Yb(3)–Sn(2)	3.533(1)	×2
Yb(1)–Ni(1)	3.403(2)	×4	Yb(3)–Sn(3)	3.3765(9)	×4
Yb(2)–Sn(1)	3.2658(9)	×4	Yb(3)–Ni(1)	3.593(1)	×4
Yb(2)–Sn(2)	3.178 (1)	×2	Ni(1)–Sn(2)	2.523(1)	×2
Yb(2)–Sn(3)	3.069(1)	×2	Ni(1)–Sn(3)	2.588(1)	×1
Yb(2)–Ni(1)	3.200 (1)	×4	Ni(1)–Sn(1)	2.592 (1)	×1
Sn(1)–Sn(1)	2.936(1)	×1	Ni(1)–Sn(1)	2.645 (2)	×1
Sn(1)–Sn(2)	3.183(1)	×2	Sn(2)–Sn(2)	3.213(1)	×2
			Sn(3)–Sn(3)	2.798(2)	×1
$Yb_7Ni_4Sn_{13}$					
Yb(1)–Sn(1)	3.403(1)	×4	Yb(2)–Sn(1)	3.3800(6)	×2
Yb(1)–Sn(2)	3.2214(5)	×8	Yb(2)–Sn(2)	3.3046(9)	×1
Yb(1)–Ni(1)	3.354(1)	×4	Yb(2)–Sn(3)	3.1489(6)	×2
Yb(3)–Sn(1)	3.5231(6)	×4	Yb(2)–Sn(3)	3.2783(6)	×2
Yb(3)–Sn(2)	3.5515(7)	×2	Yb(2)–Sn(4)	3.4614(4)	×2
Yb(3)–Sn(3)	3.3063(6)	×4	Yb(2)–Ni(1)	3.381(1)	×2
Yb(3)–Ni(1)	3.627(1)	×4	Sn(1)–Sn(3)	2.855(1)	×1
Ni(1)–Sn(2)	2.5045(7)	×2	Sn(1)–Sn(2)	3.2542(7)	×2
Ni(1)–Sn(3)	2.523(2)	×1	Sn(2)–Sn(2)	3.238(1)	×2
Ni(1)–Sn(1)	2.573(2)	×1	Sn(3)–Sn(4)	3.1793(7)	×1
Ni(1)–Sn(1)	2.599(2)	×1			

3. Results and discussion

3.1. Structure descriptions

$Yb_5Ni_4Sn_{10}$ belongs to the $Sc_5Co_4Si_{10}$-type structure, which is also known for other relevant germanide, such as $RE_5Rh_4Ge_{10}$ (*RE*=Y, Gd–Tm, Lu) [54,55]. Its structure features a 3D [Ni_4Sn_{10}] framework composed of three types of 1D channels, propagating along the *c*-axis, in which the Yb atoms are situated (Fig. 1a).

The biggest channels in the structure are built from stacked alternating planar octagonal and square rings interconnected via Ni–Sn and Sn–Sn bonds, in which the octagons are comprised from alternating four Ni(1) and four Sn(1) atoms, and the square rings are composed of four Sn(2) atoms. Yb(1) atoms are sitting in the center of octagonal rings (Fig. 2a). The second tunnel is based

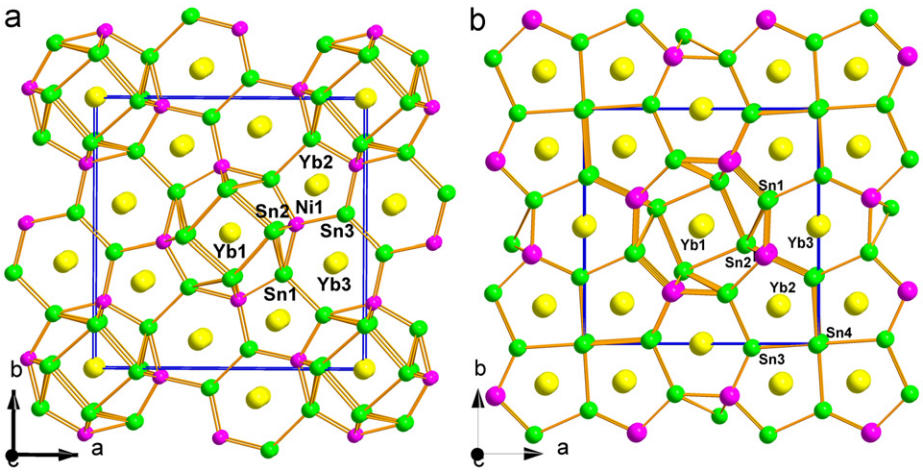

Fig. 1. View of the structures of $Yb_5Ni_4Sn_{10}$ (a) and $Yb_7Ni_4Sn_{13}$ (b) along the *c*-axis. The ytterbium, nickel, and tin atoms are drawn as yellow, purple, and green spheres, respectively. (For interpretation of the references to the color in this figure legend, the reader is referred to the web version of this article.)

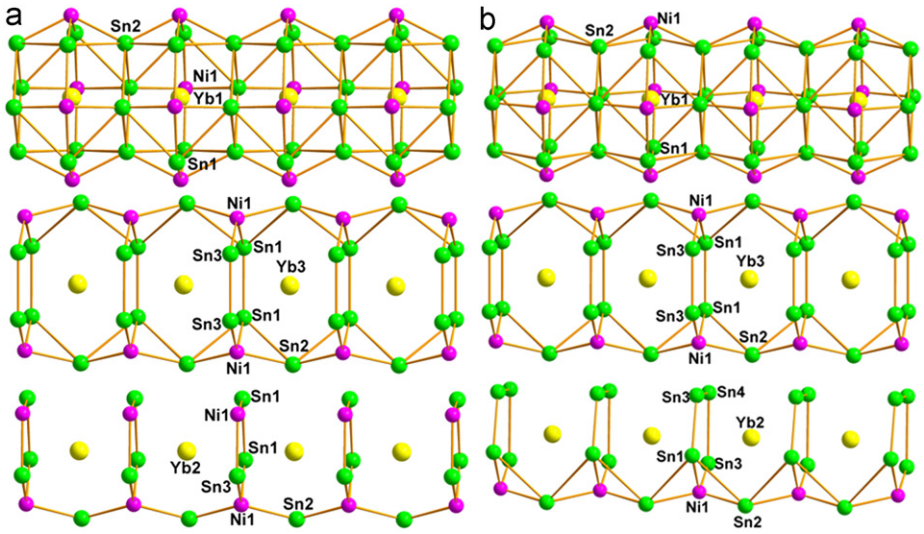

Fig. 2. The octagonal, hexagonal, pentagonal rings and their interconnection to form the corresponding tunnels running down the *c*-axis in $Yb_5Ni_4Sn_{10}$ (a) and $Yb_7Ni_4Sn_{13}$ (b). The situated Yb atoms are also highlighted.

on planar [Ni_2Sn_4] hexagonal rings. In these, Sn(1)–Sn(1) and Sn(3)–Sn(3) dimers are interconnected by two Ni(1) atoms to form distorted hexagonal rings that are stacked parallel and bridged by Sn(2) atoms along the *c*-axis (Fig. 2a). In contrast to the octagonal tunnels, here, the Yb(3) atoms are sandwiched between the hexagonal rings. The final structural feature is the pentagonal channels based on [Ni_2Sn_3] 5-membered rings, which are interconnected by Sn(2) atoms along the *c*-axis (Fig. 2b). Similar to the Yb(3) atoms in the hexagonal tunnels, Yb(2) atoms are also sandwiched between the pentagonal rings. The Ni–Sn bond distances fall in the range of 2.523(1)–2.645(2) Å, which are comparable with the sum of the covalent radii of 2.64 Å ($r_{Ni}+r_{Sn}$) [56], indicating strong Ni–Sn interactions. The Sn–Sn bond distances are in the range of 2.798(2)–3.213(1) Å, which are in accordance with those reported in related compounds [57–61].

Yb(1) atom is surrounded by 12 Sn atoms and four Ni atoms whereas Yb(2) atom has four Ni atoms and eight Sn atoms as its neighbors. Yb(3) atom located at the hexagonal tunnel is in contact with four Ni atoms and 10 Sn atoms. The Yb–Ni distances are in the range of 3.200(1)–3.593(1) Å, which are significantly longer than those in $YbNi_2Sn$ (2.752 Å) and $Yb_{1-x}Ni_4Sn_{1+x}$ (2.898 Å) [36,37]. This is mainly due to the Yb–Ni interaction in $Yb_5Ni_4Sn_{10}$ is much weaker compared with those in the Ni-rich phases. The Yb–Sn distances fall in the range of 3.069(1)–3.533(1) Å, which are comparable with those reported in $Yb_4Cu_2Sn_5$ [62], Yb_3CoSn_6 [63], and YbZnSn [64].

$Yb_7Ni_4Sn_{13}$ is isostructural with $Yb_7Co_4InGe_{12}$ [65], in which the Co sites are replaced by Ni atoms and all the In, Ge sites are substituted by Sn atoms. Its structure features a 3D [Ni_4Sn_{13}] framework composed of three 1D channels along the *c*-axis that are filled by Yb atoms (Fig. 1b). Similar to that in $Yb_5Ni_4Sn_{10}$, the biggest channels are composed of stacked alternating planar octagons and square rings interconnected via Ni–Sn and Sn–Sn bonds along the *c*-axis (Fig. 2b). The second hexagonal tunnels are also based on [Ni_2Sn_4] 6-membered rings composed of two Ni(1) atoms and two Sn(1)–Sn(3) dimers interconnected via Ni–Sn bonds, which are stacked parallel and connected via Sn(2) atoms along the *c*-axis (Fig. 2b). The final noteworthy structural moiety is the pentagonal channels based on [$NiSn_4$] 5-membered rings composed of one Ni(1), one Sn(1), one Sn(4) and two Sn(3) atoms interconnected via Ni–Sn and Sn–Sn bonds. The pentagonal rings extend along the *c*-axis bridged by Sn(2) atoms (Fig. 2b). The Yb(1) and Yb(3) atoms are located in the octagonal and hexagonal channels, respectively, with the same coordination environments as those in $Yb_5Ni_4Sn_{10}$. Yb(2) atoms are situated in the pentagonal tunnels and 11-coordinated by two Ni atoms and nine Sn atoms. The Yb–Ni and Yb–Sn bond lengths fall in the range of 3.354(1)–3.627(1) and 3.1489(6)–3.5515(7) Å, respectively, which are comparable with those in $Yb_5Ni_4Sn_{10}$. The Ni–Sn and Sn–Sn bond distances are in the range of 2.5045(7)–2.599(2) Å and 2.855(1)–3.2542(7) Å, respectively, which are comparable with those in $Yb_5Ni_4Sn_{10}$.

It is interesting to compare the structure of $Yb_5Ni_4Sn_{10}$ with that of $Yb_7Ni_4Sn_{13}$. Both structures feature three types of 1D tunnels: octagonal, hexagonal and pentagonal tunnels. Both the octagonal and hexagonal tunnels are similar in the two compounds, whereas the pentagonal tunnels are composed of planar [Ni_2Sn_3] and [$NiSn_4$] rings, respectively, in $Yb_5Ni_4Sn_{10}$ and $Yb_7Ni_4Sn_{13}$. Similar to that of $Sc_5Co_4Si_{10}$ [54], the structure of $Yb_5Ni_4Sn_{10}$ can also be considered as built from three types of 1D columns: [$YbSn_8$] (Cu_3Au-type), [Yb_4Sn_2] (AlB_2-type), and interbedded [$NiSn_4Yb_4$] ($BaAl_4$-type) columns (Fig. S1a). Similarly, the structure of $Yb_7Ni_4Sn_{13}$ can be built from four types of 1D columns: [$YbSn_8$] (Cu_3Au-type), [Yb_4Sn], [Yb_3Sn] (AlB_2-type) and [$NiSn_4Yb_4$] ($BaAl_4$-type) columns (Fig. S1b).

3.2. Physical properties

The plots of the molar magnetic susceptibility χ_m of crystalline samples for the title compounds as a function of temperature are presented in Fig. 3. $Yb_5Ni_4Sn_{10}$ exhibits a weak paramagnetic behavior in the temperature range of 50–300 K. Below 50 K, the small upturn of χ_m maybe come from the presence of small amount of paramagnetic impurities. Such phenomena have also been observed in many Yb containing phases [66–67]. Linear fitting of the susceptibility data in the temperature range of 50–300 K gives an effective moment of 0.14 μ_B/Yb, which is much smaller than the effective moment of 4.54 μ_B/Yb expected from Hund's rules for a Yb^{3+} and slightly larger than $\mu_{eff}=0$ for a close-shell Yb^{2+}. A reasonable interpretation of this data is that Yb atoms are divalent and there are small amounts of paramagnetic Yb^{3+} impurities in the sample. If all the impurities are assumed to be Yb^{3+}, an estimation of the volume fraction of Yb^{3+} in the sample can be made. With this assumption, the low-temperature susceptibility can be understood as arising from the presence of

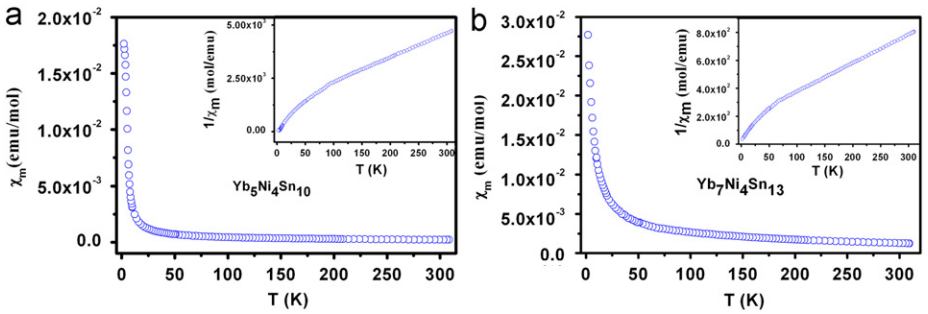

Fig. 3. Temperature dependencies (5–300 K) of the magnetic susceptibility (χ_m) of $Yb_5Ni_4Sn_{10}$ (a) and $Yb_7Ni_4Sn_{13}$ (b). The inset shows $1/\chi_m$ as a function of the temperature.

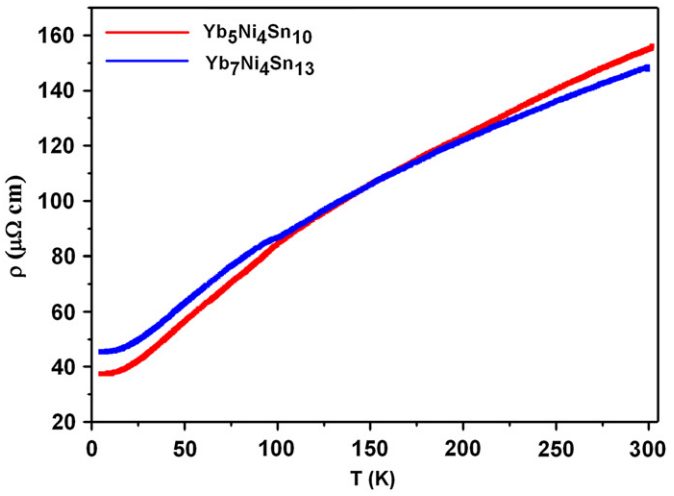

Fig. 4. Temperature dependencies of the electrical resistivities of $Yb_5Ni_4Sn_{10}$ and $Yb_7Ni_4Sn_{13}$.

$< 0.1\%$ Yb^{3+}. These considerations strongly indicate that the Yb cations are divalent in $Yb_5Ni_4Sn_{10}$. $Yb_7Ni_4Sn_{13}$ also exhibits a weak paramagnetic behavior in the temperature range of 70–300 K with small upturn of χ_m below 70 K derived from small amount of Yb^{3+} impurities. Simple calculations of the susceptibility data in the temperature range of 70–300 K gave an effective moment of 0.25 μ_B/Yb, which is slightly larger than μ_{eff}=0 for the close-shell Yb^{2+}. This number indicates that the Yb cations should be also divalent in $Yb_7Ni_4Sn_{13}$.

The results of resistivity measurements for the two compounds are presented in Fig. 4. Both compounds show typical metallic-like behavior. Their resistivities at room temperature are of the order of 130–150 μΩ cm, and it decreases continuously up cooling and reaches 30–50 μΩ cm at 5 K. These values are comparable with those for *RE*NiSn$_4$ (*RE*=Gd–Tm, Lu) [23] and $RE_9Ni_{24}Sn_{29}$ (*RE*=Y, La–Nd, Sm, Gd, Tb) phases [30].

3.3. Electronic structure calculations

To investigate the nature of band characters and transport properties of the two compounds, we carried out electronic structure calculations by using the FPLAPW method. No obvious spin splitting was observed in both compounds. The calculated total density of states (DOS) and partial density of states (PDOS) from each element with no spin-polarization for $Yb_5Ni_4Sn_{10}$ and $Yb_7Ni_4Sn_{13}$ are shown in Fig. 5. It is seen that their Fermi levels fall in the nonzero area with large density of states, indicating that both compounds are metallic. In both cases, the narrow peaks just below the Fermi level belong to the Yb 4*f* states, which are almost fully occupied. The Yb 6*s* states are mainly located above the Fermi level. Furthermore, the calculations converge to theoretical saturation moments of almost 0 μ_B for all the Yb cations in both compounds. Hence the Yb cations are most likely in an oxidation state of +2, which are in accordance with the results of magnetic measurements. In both cases, the states in the energy range of -10 to -5.5 eV are essentially dominated by Sn 5*s* electrons. In the region of -5 eV up to the Fermi level, the profile of projected DOS shows mixing between Ni 3*d* and Sn 5*p* states as well as small amount of Yb 4*f* states, which are mainly responsible for the metallic character of the two compounds.

Furthermore, considering the local 3*d* and 4*f* electrons in these compounds, we further perform the GGA+*U* (on-site Coulombic energy correction) type calculations to examine the correlation of *d* or *f* electrons. It is found that the density of states is unchanged except small quantitative changes for two compounds. Namely, the *U* parameter does not influence the energy and DOS of both 3*d* and 4*f* electrons. Thus, the GGA exchange correlation formation can give sufficient and reliable results.

To further check the chemical bonding, the results of the TB–LMTO–ASA calculations have been utilized for the interpretation of bonding through crystal orbital Hamilton population (–COHP) analyses as well as integrated –COHP (–ICOHP) analyses (Supplementary materials). Such calculation strategy has been effectively used in many cases [68–70]. The states just below the Fermi level are mainly from the Ni–Sn and Sn–Sn bonding interactions, which suggest that the Ni–Sn and Sn–Sn bonds are significantly contributed to the stability of the compounds. All the Ni–Sn bonds (2.50–2.65 Å) are effectively optimized at the Fermi level with largest –ICOHP values of 1.51–1.78 and 1.48–1.6 eV/bond, respectively, for $Yb_5Ni_4Sn_{10}$ and $Yb_7Ni_4Sn_{13}$, which show the strong covalent Ni–Sn bonding interactions (Fig. 6). The Sn–Sn bonds show various bonding characters depending on the bond distances. Most of the Sn–Sn bonds are fully occupied below the Fermi level corresponding to the covalent Sn–Sn bonding interactions. It should be noted that some of the Sn–Sn antibonding states around the Fermi level are also filled suggesting some weakening of Sn–Sn bonding interactions, which have been investigated in detail elsewhere [71–74]. In $Yb_5Ni_4Sn_{10}$, the shorter Sn–Sn bonds of 2.798(2) Å and 2.936(1) Å have relative large –ICOHP values of 1.29 and 1.20 eV/bond, respectively, which are much stronger than those slightly longer Sn–Sn bonds (3.183(1)–3.451(1) Å) with –ICOHP values of 0.24–0.59 eV/bond. Similar bonding characters are also found in $Yb_7Ni_4Sn_{13}$. It is obvious that the overlap populations are in consistent with the bond lengths. As expected, the Yb–Sn bonds (3.0–3.6 Å) are weakly bonding with small –ICOHP value of about 0.34–0.05 eV/bond, and Yb–Ni (3.2–3.7 Å) bonds are essentially nonbonding with very small –ICOHP value of 0.12 ~ -0.17 eV/bond. Hence, we can say that the covalent characters of Ni–Sn and

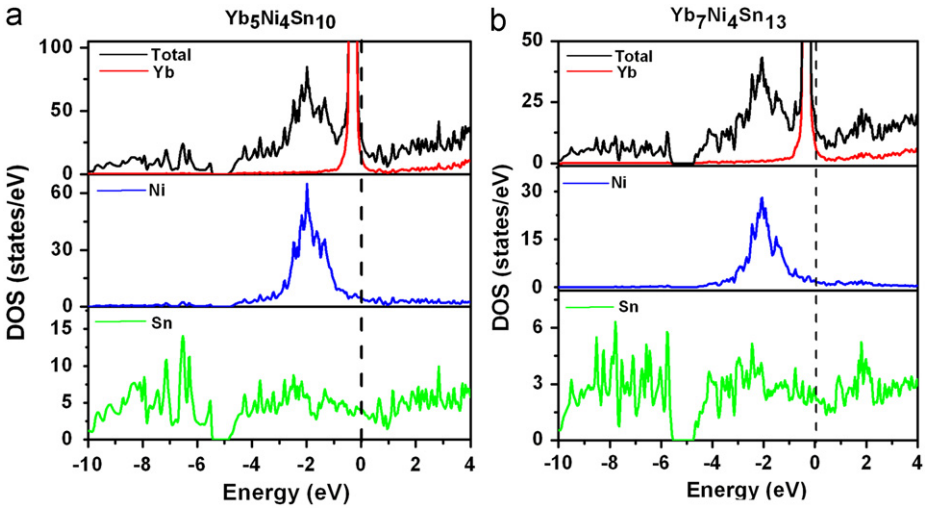

Fig. 5. TDOS and PDOS for $Yb_5Ni_4Sn_{10}$ (a) and $Yb_7Ni_4Sn_{13}$ (b). TDOS: black solid line; Yb: red; Ni: blue; Sn: green. The Fermi level is set at 0 eV. (For interpretation of the references to the color in this figure legend, the reader is referred to the web version of this article.)

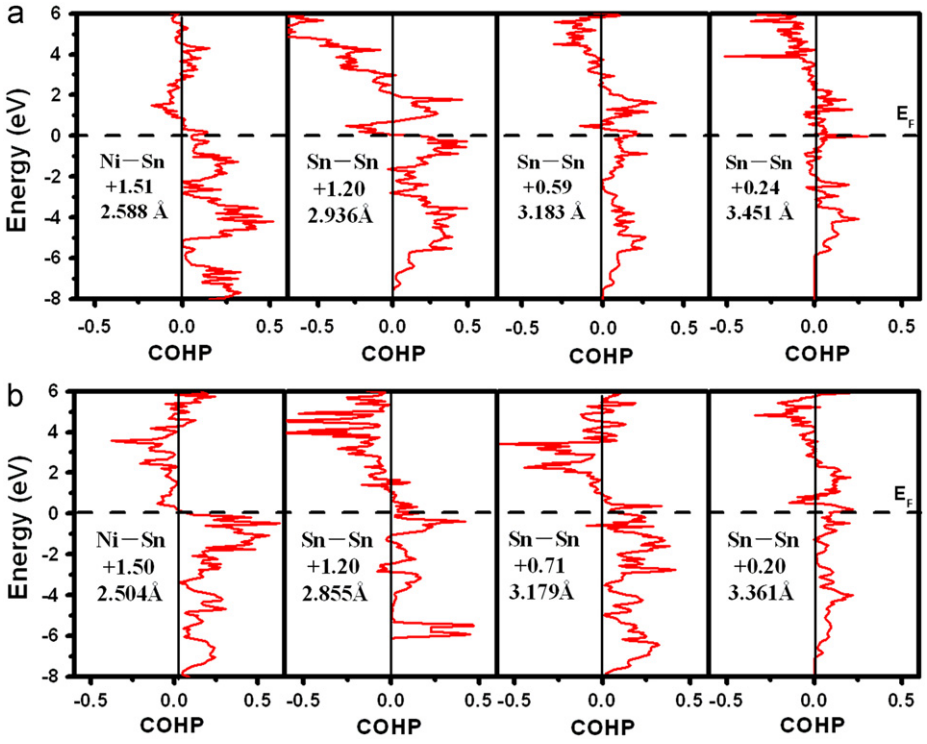

Fig. 6. Selected –COHP curves for $Yb_5Ni_4Sn_{10}$ (a) and $Yb_7Ni_4Sn_{13}$ (b). The integrated values for the overlap –ICOHP per bond up to the Fermi level (dashed line) and the corresponding distances are given.

Sn–Sn bonds are greater than those of Yb–Ni and Yb–Sn bonds. The structure of $Yb_5Ni_4Sn_{10}$ and $Yb_7Ni_4Sn_{13}$ can be considered as 3D $[Ni_4Sn_{10}]$ and $[Ni_4Sn_{13}]$ anionic framework with Yb atoms mainly as spacers, respectively.

4. Conclusions

In summary, we have successfully obtained two new ternary ytterbium nickel stannides, namely, $Yb_5Ni_4Sn_{10}$ and $Yb_7Ni_4Sn_{13}$. Their structures both feature 3D frameworks characterized by three types of 1D channels along the *c*-axis, in which all the Yb atoms are situated. Magnetic and resistivity measurements for both compounds revealed that they are weakly paramagnetic with reasonably good electrical conductivity and the Yb cations are divalent. The experimental results have been complimented by electronic structure calculations. Further research efforts will be devoted to other physical properties, such as thermoelectric properties of these compounds.

Acknowledgments

We thank the financial supports from the National Nature Science Foundation of China (Nos. 20573113, 20825104 and 20821061). We thank Prof. Shunlian Jia for help with the resistivity measurements.

Appendix A. Supplementary material

Supplementary data associated with this article can be found in the online version at doi:10.1016/j.jssc.2010.02.004.

References

[1] R. Pöttgen, Z. Naturforsch. 61b (2006) 677.
[2] M.G. Kanatzidis, R. Pöttgen, W. Jeitschko, Angew. Chem. Int. Ed. 44 (2005) 6996.
[3] R.V. Skolozdra, Stannides of the rare-earth and transition metals, in: K.A. Gschneidner, L. Eyring (Eds.), Handbook on the Physics and Chemistry of Rare Earths, vol. 24, Elsevier, Amsterdam, 1997, p. 164.
[4] D. Niepmann, R. Pöttgen, B. Künnen, G. Kotzyba, B.D. Mosel, Chem. Mater. 12 (2000) 533.
[5] G. Heymann, S. Rayaprol, J.F. Riecken, R.D. Hoffmann, U.C. Rodewald, H. Huppertz, R. Pöttgen, Solid State Sci. 8 (2006) 1258.
[6] H.-P. Liu, M. Colarieti-Tosti, A. Broddefalk, Y. Andersson, E. Lidström, O. Eriksson, J. Alloys Compd. 306 (2000) 30.
[7] S. Miraglia, J.L. Hodeau, M. Marezio, C. Laviron, M. Ghedira, G.P. Espinosa, J. Solid State Chem . 63 (1986) 358.
[8] D. Niepmann, R. Pöttgen, B. Künnen, G. Kotzyba, C. Rosenhahn, B.D. Mosel, Chem. Mater. 11 (1999) 1597.
[9] B. Chevalier, C.P. Sebastian, R. Pöttgen, Solid State Sci. 8 (2006) 1000.
[10] R. Pöttgen, R.-D. Hoffmann, R. Müllmann, B.D. Mosel, G. Kotzyba, Chem. Eur. J. 3 (1997) 1852.
[11] C.P. Sebastian, L. Zhang, C. Fehse, R.-D. Hoffmann, H. Eckert, R. Pöttgen, Inorg. Chem. 46 (2007) 771.
[12] S. Singh, S.K. Dhar, P. Manfrinetti, A. Palenzona, J. Magn. Magn. Mater. 250 (2002) 190.
[13] E.L. Thomas, H.-O. Lee, A.N. Bankston, S. MaQuilon, P. Klavins, M. Moldovan, D.P. Young, Z. Fisk, J.Y. Chan, J. Solid State Chem. 179 (2006) 1641.
[14] X.-W. Lei, G.-H. Zhong, C.-L. Hu, J.-G. Mao, J. Alloys Compd. 485 (2009) 124.
[15] F. Canepa, M. Napoletano, C. Lefèvre, G. Venturini, J. Alloys Compd. 347 (2002) 60.
[16] Y. Mudryk, A. Grytsiv, P. Rogl, C. Dusek, A. Galatanu, E. Idl, H. Michor, E. Bauer, C. Godart, D. Kaczorowski, L. Romaka, O. Bodak, J. Phys. Condens. Matter 13 (2001) 7391.
[17] O. Zaharko, L. Keller, C. Ritter, J. Magn. Magn. Mater. 253 (2002) 130.
[18] A. Aburto, E. Orgaz, Phys. Rev. B 75 (2007) 045130.
[19] P.A. Kotsanidis, J.K. Yakinthos, E. Roudaut, J. Magn. Magn. Mater. 124 (1993) 51.
[20] L. Romaka, M. Konyk, V.V. Romaka, N. Melnychenko, P. Rogl, J. Alloys Compd. 454 (2008) 136.
[21] R. Mallik, E.V. Sampathkumaran, Phys. Rev. B 58 (1998) 9178.
[22] V.K. Pecharsky, K.A. Gschneidner Jr, L.L. Miller, Phys. Rev. B 43 (1991) 10906.
[23] R.V. Skolozdra, J.S. Mudryk, L.G. Akselrud, D. Fruchart, D. Gignoux, J. Pierre, L.P. Romaka, D. Schmitt, J. Alloys Compd. 296 (2000) 303.
[24] Z.-M. Sun, D.-C. Pan, X.-W. Lei, J.-G. Mao, J. Solid State Chem. 179 (2006) 3378.
[25] S.F. Matar, B. Chevalier, O. Isnard, J. Etourneau, J. Mater. Chem. 13 (2003) 916.
[26] R.V. Skolozdra, L.G. Aksel'rud, O.E. Koretskaya, L.P. Komarovskaya, Dopov. Akad. Nauk Ukr. RSR, Ser. B Geol, Khim. Biol. Nauki 1985 (1985) 24.
[27] L.P. Komarovskaya, R.V. Skolozdra, Dopov. Akad. Nauk Ukr. RSR, Ser. A Fiz-Mat. Tekh. Nauki. 47 (1985) 81.
[28] V.V. Romaka, R. Gladyshevskii, Yu. Gorelenko, J. Alloys Compd 453 (2008) L8.
[29] M.A. Zhuravleva, D. Bilc, S.D. Mahanti, M.G. Kanatzidis, Z. Anorg. Allg. Chem. 629 (2003) 327.
[30] D. Kaczorowski, K. Gofryk, L. Romaka, Ya. Mudryk, M. Konyk, P. Rogl, Intermetallics 13 (2005) 484.
[31] L. Romaka, B. Penc, S. Baran, J. Leciejewicz, A. Szytuła, N. Stüsser, J. Hernandez-Velasco, A. Zygmunt, J. Alloys Compd. 343 (2002) 66.
[32] R.-D. Hoffmann, R. Pöttgen, D. Kussmann, R. Müllmann, B.D. Mosel, Chem. Mater. 13 (2001) 4019.
[33] M.L. Fornasini, P. Manfrinetti, D. Mazzone, P. Riani, G. Zanicchi, J. Solid State Chem. 177 (2004) 1919.
[34] P. Bonville, P. Bellot, J.A. Hodges, P. Imbert, G. Jéhanno, G. Le Bras, J. Hammann, L. Leylekian, G. Chevrier, P. Thuéry, L. D'Onofrio, A. Hamzic, A. Barthélémy, Physica B 182 (1992) 105.
[35] C. Rizzoli, P.S. Salamakha, O.L. Sologub, G. Bocelli, J. Alloys Compd. 340 (2002) 146.
[36] R.V. Skolozdra, L.P. Komarovskaya, Ukr. Fiz. Zh. 28 (1983) 1093.
[37] C. Rizzoli, O.L. Sologub, P.S. Salamakha, J. Alloys Compd. 337 (2002) L1.
[38] R.V. Skolozdra, R. Szymchak, H. Szymchak, L. Romaka, M. Baran, J. Phys. Chem. Solids 57 (1996) 357.
[39] CrystalClear version. 1. 3. 5; Rigaku Corp.: Woodlands, TX, 1999.
[40] G.M. Sheldrick, SHELXTL, Crystallographic Software Package, version 5.1; Bruker-Axs; Madison, WI, 1998.
[41] G.K.H. Madsen, P. Blaha, K. Schwarz, E. Sjöstedt, L. Nordstrom, Phys. Rev. B 64 (2001) 195134.
[42] K. Schwarz, P. Blaha, G.K.H. Madsen, Comput. Phys. Commun. 147 (2002) 71.
[43] J.P. Perdew, K. Burke, M. Ernzerhof, Phys. Rev. Lett. 77 (1996) 3865.
[44] P. Blaha, K. Schwarz, G.K.H. Madsen, D. Kvasnicka, J. Luitz, WIEN2k, in: K. Schwarz (Ed.), An Augmented Plane Wave+Local Orbitals Program for Calculating Crystal Properties, Technische Universität Wien, Austria, 2001.
[45] P.E. Blöchl, O. Jepsen, O.K. Andersen, Phys. Rev. B 49 (1994) 16223.
[46] O.K. Andersen, Phys. Rev. B 12 (1975) 3060.
[47] O.K. Andersen, O. Jepsen, Phys. Rev. Lett. 53 (1984) 2571.
[48] O.K. Andersen, O. Jepsen, D. Glötzel, in: F. Bassani, F. Fumi, M.P. Tosi (Eds.), Highlights of Condensed Matter Theory, North Holland, New York, 1985.
[49] O. Jepsen, O.K. Andersen, The Stuttgart TB-LMTO Program, Version 4.7.
[50] U. Von Barth, L. Hedin, J. Phys. C 5 (1972) 1629.
[51] W.R.L. Lambrecht, O.K. Andersen, Phys. Rev. B 34 (1986) 2439.
[52] O.K. Andersen, Phys. Rev. B 62 (2000) R16219.
[53] E. Pavarini, New J. Phys. 7 (2005) 188.
[54] H.F. Braun, K. Yvon, R.M. Braun, J. Less-Common Met. 100 (1984) 105.
[55] N.G. Patil, S. Ramakrishnan, Phys. Rev. B 59 (1999) 9581.
[56] L. Pauling, B. Kamb, Proc. Natl. Acad. Sci. (USA) 83 (1986) 3569.
[57] A.K. Ganguli, A.M. Guloy, E.A. Leon-Escamilla, J.D. Corbett, Inorg. Chem. 32 (1993) 4349.
[58] E.A. Leon-Escamilla, J.D. Corbett, Inorg. Chem. 38 (1999) 738.
[59] Z.-M. Sun, S.-Q. Xia, Y.-Z. Huang, L.-M. Wu, J.-G. Mao, Inorg. Chem. 44 (2005) 9242.
[60] V. Hlukhyy, S. Eck, T.F. Fässler, Inorg. Chem. 45 (2006) 7408.
[61] V. Hlukhyy, F. Raif, P. Claus, T.F. Fässler, Chem. Eur. J. 14 (2008) 3737.
[62] M.L. Fornasini, G. Zanicchi, D. Mazzone, P. Riani, Z. Kristallogr, NCS 216 (2001) 21.
[63] X.-W. Lei, G.-H. Zhong, M.-J. Li, J.-G. Mao, J. Solid State Chem. 181 (2008) 2448.
[64] R. Pöttgen, P.E. Arpe, C. Felser, D. Kuβmann, R. Müllmann, B.D. Mosel, B. Künnen, G. Kotzyba, J. Solid State Chem. 145 (1999) 668.
[65] M. Chondroudi, M. Balasubramanian, U. Welp, W.-K. Kwork, M.G. Kanatzidis, Chem. Mater. 19 (2007) 4769.
[66] S.-Q. Xia, S. Bobev, J. Am. Chem. Soc. 129 (2007) 4049.
[67] S. Bobev, V. Fritsch, J.D. Thompson, J.L. Sarrao, B. Eck, R. Dronskowski, S.M. Kauzlarich, J. Solid State Chem. 178 (2005) 1071.
[68] A.-V. Mudring, J.D. Corbett, J. Am. Chem. Soc. 126 (2004) 5277.
[69] S. Bobev, E.D. Bauer, J.D. Thompson, J.L. Sarrao, G.J. Miller, B. Eck, R. Dronskowski, J. Solid State Chem. 177 (2004) 3545.
[70] X.-W. Lei, G.-H. Zhong, L.-H. Li, C.-L. Hu, M.-j. Li, J.-G. Mao, Inorg. Chem. 48 (2009) 2526.
[71] S.-J. Kim, S.-Q. Hu, C. Uher, M.G. Kanatzidis, Chem. Mater. 11 (1999) 3154.
[72] S.-J. Kim, M.G. Kanatzidis, Inorg. Chem. 40 (2001) 3781.
[73] S.-M. Park, S.-J. Kim, M.G. Kanatzidis, J. Solid State Chem. 177 (2004) 2867.
[74] S.-M. Park, S.-J. Kim, M.G. Kanatzidis, J. Solid State Chem. 175 (2003) 310.